CHAPTER 2:

REVIEW OF LITERATURE

CHAPTER 2

REVIEW OF LITERATURE

This chapter contains a critical review of the existing literature on the techniques of achieving the microstructure and the mechanical properties in DP steels. The outstanding mechanical properties of DP steels have been stated. Furthermore, different types of wear have been discussed, elaborating on the erosive wear process and the mechanism of erosion in both ductile and brittle materials. The steady state erosion rate models have been described to understand the critical property of the materials causing erosion. A comprehensive review of the erodent properties, such as erodent shape, size, flow rate, impact velocity and angle, and target material properties on the erosive wear process, are also included in this chapter. It is followed by an exhaustive survey on the various aspects of erosive wear behavior of metals, in general, and of steels, in particular. In the end the formulation of the problem and the objectives of the research are presented.

2.1 DUAL PHASE STEEL AND THEIR PROPERTIES

Dual phase steels exhibit a microstructure that comprises islands of martensite surrounded by a soft ferrite matrix. The designation “dual phase” primarily denotes the coexistence of two phases, ferrite and martensite, within the microstructure, although there may be minor amounts of retained austenite, bainite, and/or pearlite as well.

2.1.1 Different Phases of Steel

Ferrite: Ferrite, characterized by its soft and low-strength properties, attains good ductility and formability when it possesses a fine grain size. Due to its bcc (body-centered cubic) crystal structure, ferritic steels undergo a shift from ductile to brittle behaviour as temperature decreases or strain rate increases.

Austenite: Gamma iron, much like alpha iron, refers exclusively to the FCC (face-centered cubic) structure of pure iron, which remains stable within the temperature range of 910°C to 1394°C. In the case of heat-treatable steels, austenite serves as the primary phase from which all transformation products originate, contributing to the versatility and commercial utility of ferrous alloys.

Delta ferrite: Delta iron represents the bcc (body-centered cubic) structure of pure iron, maintaining stability from temperatures above 1,394°C up to its melting point at 1,538°C. In contrast, delta ferrite signifies a stable solid solution of one or more elements within the bcc iron lattice at high temperatures.

Cementite: In iron, carbon can be found in two forms: cementite or graphite. Cementite is a compound composed of iron and carbon, represented by the formula Fe_3C, and it possesses an ortho-rhombic crystal structure. Cementite, also known as iron carbide, contains around 6.67% carbon, which corresponds to the formula Fe_3C.

Pearlite: Pearlite is a composite material consisting of ferrite and cementite, where these two phases develop from austenite in alternating lamellar pattern. The formation of pearlite requires a relatively gradual cooling process from the austenite region and is

influenced by the composition of the steel. In pearlitic steels, as the distance between the layers within the structure diminishes, both strength and toughness tend to increase.

Bainite: Bainite is a meta-stable structure resembling laths and consists of ferrite and cementite. It emerges from austenite at temperatures below the range at which pearlite develops but above the point where martensite begins to form. Bainite is typically categorized into upper bainite and lower bainite. Upper bainite takes shape isothermally or during continuous cooling at temperatures just below the threshold for bainite formation. In contrast, lower bainite forms at even lower temperatures, extending down to the Ms temperature.

Martensite: Martensite emerges when the cooling process from the austenitizing temperature occurs rapidly. It's essential to note that martensite does not represent an equilibrium phase in steel. The steel's hardenability dictates its capacity to generate martensite, a factor reliant on both section size and the rate of quenching. In low carbon steels, "lath" martensite is produced, while high carbon steels yield "plate" martensite, which is sometimes erroneously referred to as "acicular" martensite.

The dual phase steels possess various advantages over single phase steels:

- Excellent balance of ductility, high tensile strengths, easy cold formability, and very good crash energy-absorption.
- Dual phase steel’s High early-stage hardening makes DP steel resistant to local necking due to strain redistribution-providing highly uniform elongation.
- Dual phase steel’s low yield-to tensile strength ratio creates high global formability combined with good weld ability.

2.1.2 Types of Dual Phase Steels

DP steels are produced by heating low/medium carbon steel into two phase ferrite-austenite ($\alpha+\gamma$) region of Fe-C phase diagram, followed by rapid cooling to transform austenite (γ) into martensite, resulting in a structure of ferrite and martensite. **DP** steels are of two types.

2.1.2.1 Plain Carbon Dual Phase Steels

These steels are low or medium carbon steels having no alloying elements [12]. Due to the absence of alloying elements, these steels have poor hardenability.

2.1.2.2 Alloyed Dual Phase Steels

The chief alloying elements are manganese and silicon. Manganese is roughly around 1.5 pct. and silicon is in the range of 1 pct. Other alloying elements like chromium, vanadium and molybdenum are in small amounts. Due to higher hardenability of these steels, dual-phase structure can be obtained by simple air cooling from intercritical region in relatively thicker sections [13–15].

2.1.3 Development of Dual Phase Microstructure

There are two methods mainly used for developing dual phase microstructure in steels, namely, (a) intercritical annealing and (b) direct hot rolling technique.

2.1.3.1 Intercritical Annealing

Dual phase microstructure in steels may be developed by heat treatment of either continuous intercritical annealing or box-annealing. The continuous annealing technique is mostly

used because of higher production rates and better uniformity in properties. The flexibility of using either low carbon steel strips or low alloy steel is also an added advantage of this technique. However, box-annealing has also been used where continuous annealing facilities are not available [16–18].

In the continuous annealing technique (Fig. 2.1), the steel strip is heated for a short time (1-2 minutes) in intercritical temperature range, to form ferrite-austenite mixtures. This is followed by rapid cooling so as to allow the transformation of austenite into martensite. The actual cooling rate depends on the sheet thickness and quenching conditions on a given production line. Hence, the steel compositions need to be adjusted to obtain the hardenability needed for the sheet thickness at the given cooling rate).

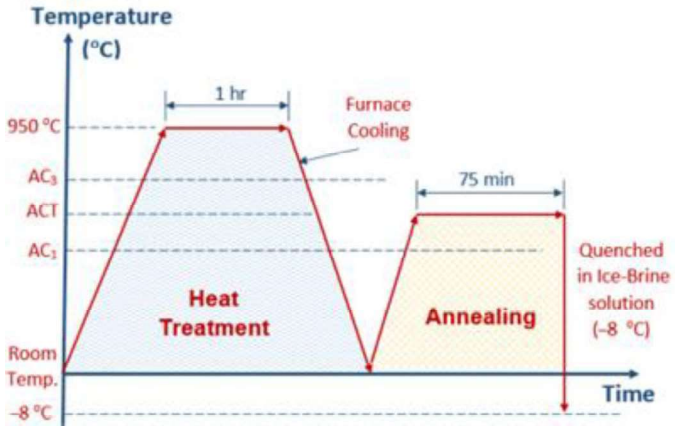

Figure 2.1 Schematic representing the intercritical annealing heat treatment routes to develop high strength steel [19]

In the box-annealing technique, similar heat treatment is carried out but the duration of annealing is relatively much longer (~ 3 hours) and the cooling rates are slower (20°C/ hr). Due to this slow cooling rate, there is a need to have much higher level of alloying in steels to achieve the desired hardenability. For this annealing technique, 2.5 pct.

manganese steels containing appreciable amounts of silicon and chromium have been proposed [18,20].

2.1.3.2 Direct Hot Rolling Technique

In addition to the use of intercritical annealing heat treatment, DP steels have also been produced by direct hot rolling method or in the as-rolled conditions by carefully controlling the continuous-cooling transformation characteristics of the steels [21,22]. This essentially requires the addition of substantial amounts of silicon, chromium and molybdenum in addition to about 1.0 wt. pct. manganese. In this method, the strip is allowed to cool rapidly on the run out table for about 10 seconds, after the last roll pass on a hot strip mill. At this stage, a large amount of polygonal ferrite (about 80 pct.) forms but the formation of pearlite is suppressed and the remaining islands of carbon enriched austenite transform to martensite during the cooling of the strip in air. A desired type of continuous cooling transformations diagram is shown in Fig. 2.2 [23].

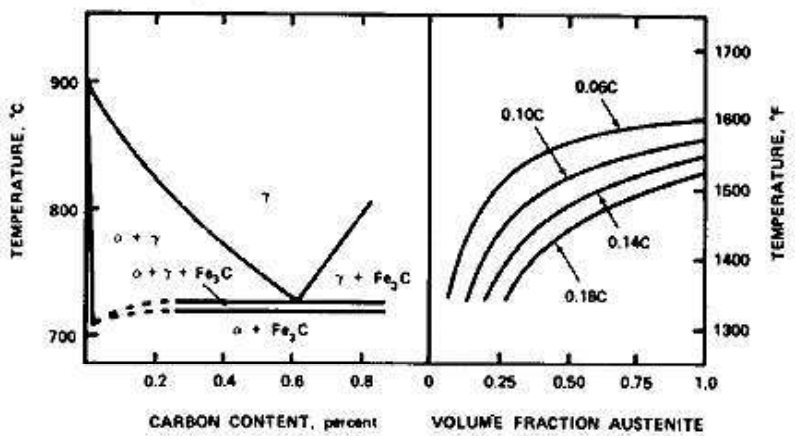

Figure 2.2 Estimated equilibrium phase diagram and volume fraction austenite at intercritical temperatures [23]

Production of DP steels by direct hot rolling has the advantage of saving energy costs by eliminating a heat treatment step. Also, DP steels can be produced when continuous-annealing facilities are not available. However, balanced against these advantages are the disadvantages of higher alloy cost and more variability in the properties in the production route of direct hot rolling. Seen against this background, the continuous annealing followed by rapid quenching seems to be the best bet for producing DP steels. However, there are certain limitations, which put restrictions on the size of the sheets to be used. The main problem for the application of dual phase plain carbon steel is its material dimension limited by insufficient hardenability.

2.1.4 Mechanical Properties of Dual Phase Steels

Dual phase steels exhibit some unique properties, which are as follows:

(i) Continuous yielding behavior i.e. absence of yield point phenomenon.

(ii) A low 0.2% offset yield strength (~340 MPa) and a high tensile strength (~ 690 MPa).

(iii) A high rate of work hardening.

(iv) High uniform and total elongation (ductility).

2.1.4.1 Continuous Yielding of Dual Phase Steel

Moinuddin Sirdar Rashid, 1976; Dabkowski & Speich, 1977 have illustrated that Ferrite-martensite DP steels typically do not exhibit a yield point phenomenon due to the combined effect of high residual stresses and a significant density of mobile dislocations formed in the ferrite phase surrounding the martensite islands. These stresses and dislocations are generated during the transformation of austenite to martensite, which

involves a volume expansion of 2-4 percent. The ferrite phase undergoes plastic deformation to accommodate this expansion in volume. As a result, when deforming the DP steel, plastic flow initiates simultaneously at multiple locations within the specimen, effectively suppressing the occurrence of discontinuous yielding or the yield point phenomenon. Moreover, the absence of a yield point in these steels prevents the formation of Luder bands and ensures a favorable surface finish after the forming process [13,24].

2.1.4.2 Yield Strength and Tensile Strength

Based on the simple composite strengthening theory, it is expected that the strength of DP steel should increase when either the volume fraction or the strength of martensite phase is increased [15,25,26]. If equal strains are assumed in both phases (which is far from reality in actual practice as strain should be more in softer ferrite phase), the variation of yield strength, σ_y, and tensile strength, σ_T, of ferrite-martensite mixtures when volume fraction of martensite is V_m, can be deduced from the "Law of Mixtures", as,

$$\boldsymbol{\sigma_y = \sigma_{y,\ \alpha}\,(1 - V_m) + \sigma_{y,\ m}\,V_m} \qquad \text{Eq. 2.1}$$

$$\boldsymbol{\sigma_T = \sigma_{T,\ \alpha}\,(1 - V_m) + \sigma_{T,\ m}\,V_m} \qquad \text{Eq. 2.2}$$

Where, $\sigma_{y,\ \alpha}$ and $\sigma_{y,\ m}$ are the yield strengths and $\sigma_{T,\ \alpha}$ and $\sigma_{T,\ \mathrm{m}}$ are the tensile strength, respectively of ferrite and martensite phases. V_m and (1-V_m) are respectively the volume fractions of martensite and ferrite phases. G. Davies, 1978 in his studies on DP steels having 1.5 wt. pct. manganese has shown that these two equations are obeyed over the entire range of volume fraction [27]. But Speich et al., 1981 while studying the effect of

volume fraction and carbon content of martensite on the yield and tensile strength, reported a linear relationship between strength and volume fraction of martensite only over a limited range of martensite volume fraction (50 pct.). Beyond this value the variation is non-linear [15].

Nath et al., 1993 developed a single-particle model based on shear lag analysis to determine the theoretical tensile strength of the DP steels while taking into account the shape of the embedded second phase particles and the work hardening term. They assumed the martensite islands to be of cylindrical shape (radius *r* and half-length *l*) with the hemispherical ends and arrived at the following expression for the ultimate tensile strength of the dual phase steels,

$$\sigma_{u,\ c} = \sigma_{u,\ m}\left(1 - \frac{r}{l}\right)V_m + \sigma_{u,\ f}\left(1 - (\frac{2}{3}\frac{r}{l} - 1)V_m\right) + KG\sqrt{\frac{bV_m\varepsilon}{0.41D_m}} \qquad \text{Eq. 2.3}$$

Where, $\sigma_{u,\ c}$, $\sigma_{u,\ m}$ and $\sigma_{u,\ f}$ are the ultimately tensile strengths of the DP steel, martensite phase and matrix (ferrite), respectively, *b* is the burgers vector of the matrix dislocations, V_m is the volume fraction of second phase particles, D_m is average particle size of martensite, ε is the true strain and *K* is a constant of order unity. Using this relation, they have shown theoretical UTS of the DP steel is in good agreement with the experimental measured strength, but when the shape of the martensite particle is assumed spherical, then the theoretical strength predicted by the shear-lag analysis do not conform with experimental values of strength observed in DP steels.

The three factors contributing to strengthening of DP steels are: (1) strain hardening of ferrite due to strain from martensitic transformation (2) the constraint on plastic

deformation of ferrite by adjacent martensite during deformation and (3) load transfer by ferrite to martensite enabling the latter to carry load as in composite materials [25].

2.1.4.3 High Rates of Work Hardening

Balliger & Gladman, 1981 have indicated that the work hardening rates are directly associated with the amount of martensite and size of martensite particles or islands. After carrying out TEM examinations of deformed dual phase structures it has been shown by them that martensite remains undeformed, even at relatively high strains and polygonal ferrite flows extensively around the martensite.

Ashby, 1966 [28], has proposed a theory of work hardening where the second phase particles act as the barrier in the movement of dislocations and has shown that the rate of work-hardening $d\sigma / d\varepsilon$ is given by,

$$\frac{d\sigma}{d\varepsilon} = \mathbf{0.78}\, KG\, \frac{b^{-1/2}}{\varepsilon^{-1/2}} \sqrt{\frac{V_m}{D_m}} \qquad \text{Eq. 2.4}$$

Where, σ is the true stress, G is the shear modulus of the matrix and b is the burgers vector of the matrix dislocations. V_m is the volume fraction of second phase particles; D_m is average particle diameter and K is a constant of order unity.

This expression indicates that at a given strain, the work hardening rate is directly proportional to the square root of the volume fraction of hard particles and inversely proportional to the square root of mean particle diameter. Therefore, the work hardening rate increases with increasing volume fraction of martensite and with decreasing martensite particle size. In terms of relative importance, the volume fraction of

martensite is more important in controlling the level of strength, while the martensite island size is more important in determining the work hardening rate and, therefore, the uniform elongation at a given strength level [29].

2.1.4.4 High Uniform and Total Elongation (Ductility)

The capability of withstanding plastic deformation is an important property of engineering materials. In fact, it reflects the ability of a material to avoid localized failure during loading. This property commonly referred as the "ductility" of the material, is indicated by the percentage strain at fracture. Thus, higher percentage elongation means higher ductility. DP steels have high total and uniform elongation; hence these steels have high ductility. The various factors influencing the ductility of DP steels are:

(i) Volume fraction of martensite

(ii) Size of martensite island

(iii) Alloy content of ferrite

(iv) Carbon content of ferrite

(v) Amount of epitaxial ferrite and retained austenite.

Assuming that in a mixture of ferrite and martensite phases in dual phase structure, the strains are equal in each phase, Milieko (1969) has evaluated uniform strain, ε_u for a composite from the values of K and n for each of the phases. Davies, 1978 has also used this theory to interpret his results and concluded that there is a good agreement between the experimental values and the values calculated by the Milieko's theory [30]. However, Speich et al., 1981, and M S Rashid, 1979, have shown that

power law relationship between stress and strain is not followed for DP steels because the strains in the two phases of ferrite and martensite, are widely different [15,31].

2.2 WEAR AND ITS TYPES

The progressive loss of substance from the investigating surface of a body occurring as a consequence of the interfacial rubbing process is called wear [32]. It is the consequence of the way in which surfaces come into contact. The process begins at highly stressed localized contact points. The process is complex and can follow several mechanisms depending on the composition and properties of the surface, surrounding environment, and forces involved. Wear may be classified on the basis of appearance of the worn parts or mechanisms and conditions, which prevail during material removal. The types of wear classified according to the wear mechanisms and conditions are: (i) adhesive wear (ii) adhesive wear (iii) erosive wear (iv) fretting wear (v) fatigue/delamination wear and (vi) corrosive /oxidative wear [1].

Adhesive wear is associated with low sliding velocity, small load and smooth surfaces. This is a universal type of wear that can occur in every machine and is hard to be eliminated but can only be reduced. Adhesion processes involve the interaction of asperities on two opposing surfaces in relative motion. When the asperities come in close contact, they may weld together, forming a bond at the junction, which has rupture strength greater than the yield strength of one of the contacting solids. At the contact points, the adhesive bond is stronger than the cohesive bond of the weaker material of the pair. Normally, adhesion occurs when two similar chemical composition metals are

in contact or contact surface are free from oxide layer. In such a case fracture may take place in one of the asperities resulting in transfer of material from one contacting body to other.

Abrasive wear occurs when two surfaces, one of which is harder and rougher than the other, are in sliding contact. Abrasive wear is the removal or the displacement of material from one surface by the harder asperities of another surface or by harder, loose particles. This type of wear is dangerous because it can occur suddenly with introduction of a contaminant and may lead to high wear rates and extensive damage to the surfaces.

Erosive wear is a combined process of repeated deformation and cutting. When a solid surface is gradually worn away by the action of fluids and particles, it is called erosion. Erosion of materials can take place under four different conditions: (1) impingement of solid particles against a solid surface, (2) impingement of liquid droplets against a solid surface, (3) flow of hot gases over a solid surface and (4) cavitation at a solid surface in liquid media. The most important form of erosion is that caused by solid particle impingement.

Fatigue/delamination wear refers to the cyclically repeated imposition of a stress state on the surface of a component, inducing a small degree of mechanical damage in the surface and subsurface regions with each stress pulse. Ultimately, the damage accumulation leads to failure by deformation and/or fracture at the surface.

Corrosive wear is the synergistic effect of chemical reaction at a surface with any of the mechanical wear mechanisms. In a corrosive environment sliding surface experience corrosive wear. However, in some cases the reaction layer may protect the surface or even act as a lubricant.

2.3 EROSIVE WEAR OF METALS

Erosion is derived from the Latin word ‘rodere’ which means ‘gnaw’. The study of erosion has long history and starts with some popular names like Reynolds, 1873, who wrote an article on sandblasting [33]. Famous tragedy of Brooklyn Bridge which was constructed in 1970 marked the witness of erosion in human history for the first time. Another hazardous incident due to erosion happened during the revolution in Iran in 1980, to rescue the American hostages a mission has been assigned to US military. The mission didn't work out since the sent helicopters broke down as they were forced to fly close to the ground through a sandstorm. To avoid Iranian radar, the helicopters had to fly very low, and the weather was worse than expected. The erosion of the leading edges of the turbine blades and in the helicopter engines by the sand caused the mission to fail (Fig. 2.3).

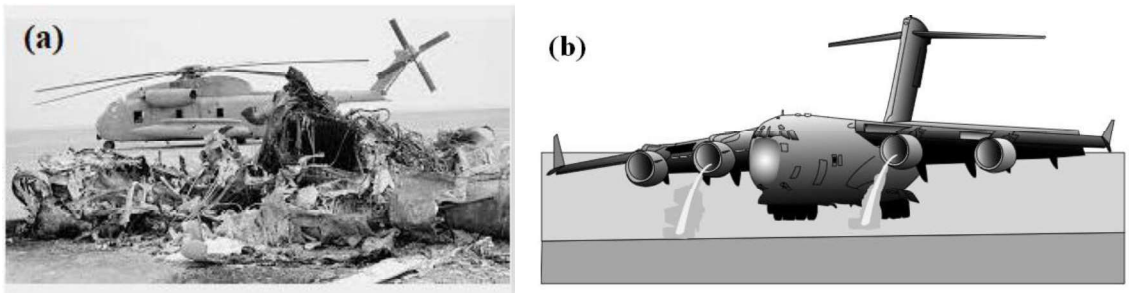

Figure 2.3 (a) Failed helicopter in the war and (b) Ingestion of dust at a runway in a desert [33]

2.3.1 Solid Particle Erosion

Solid particle erosion (SPE) is a wear process in which loss of material results from the surface by the impact of tiny solid particles causing highly localized stresses. Erosion

resulting from solid particle impact is a problem of considerable practical significance, which can result in failure of components in turbines, heat exchanger tubes, and other energy conversion systems. At the same time, it should be recognized that erosion has some beneficial aspects, for example, abrasive water jet machining, shot peening, sandblasting, ultrasonic cleaning, etc. During solid particle erosion the particles impacting on the surface also get rebounded. The contact force exerted by the surface decelerates the particles. The loss of material is defined in terms of erosion rate (E), as the ratio of the mass of material removed per unit mass of the erodent material. E is related to the impact velocity by the power law equation given below [34]:

$$\boldsymbol{E = kV^n} \qquad \text{Eq. 2.5}$$

Where, k is erosion rate constant, V, the Impact velocity and n, the velocity exponent the (3 to 3.5 for metals)

2.3.2 Models for Erosion of Materials

It is broadly agreed that the material removal occurs by extensive plastic shear. However, the steady state erosion rate models to understand the critical property of the materials causing erosion is required. Several models are facilitated by researchers, on the basis of different modes of erosion.

2.3.2.1 Cutting Models

Iain Finnie, 1959 expressed that the solid particle impact velocity and target material properties accounts for the erosion of material. Erosion in the ductile materials begins with plastic deformation and in the brittle materials by the intersection of cracks. The

Finnie cutting model is commonly expressed as:

$$\mathbf{W = k * \rho * V^2} \qquad \text{Eq. 2.6}$$

Where, W is the wear rate (mass loss per unit time), k, an erosion coefficient (material and particle-specific constant), ρ, the density of the erodent particles, and V is the impact velocity of the particles.

The model suggests that the wear rate is directly proportional to the density of the erodent particles and the square of their impact velocity. It assumes that the dominant wear mechanism in this case is cutting due to the hard and sharp nature of the erodent particles on the ductile material's surface [35].

Bitter, 1963 stated repeated deformation and cutting are the two mechanisms for erosion. Based on energy balance for a plastic-elastic collision, the erosion induced by the deformation mechanism is predicted using the following equation:

$$\boldsymbol{W_D = \frac{M\,(V_P \sin\alpha - k)^2}{2\,\delta}} \qquad \text{Eq. 2.7}$$

W_D is volume loss, M and V_p are total mass and velocity of impinging particles, respectively, (α is impact angle and k is a constant, which can be calculated from mechanical and physical properties and expresses the particle velocity at incipient erosion. δ represents the energy needed to remove a unit volume of material from the body surface and describes the plastic-elastic behaviour of the substance [36].

2.3.2.2 Localization Models

Sundararajan & Shewmon, 1983 suggested a model that considers the shear localization leading to lip formation as a function of critical strain as mentioned below:

$$\boldsymbol{\varepsilon_m = \frac{6.5\ X\ 10^{-3}\ V_P^{2.5} \rho_P^{2.5}}{C_P\ T_m^{0.75}\ H_t^{2.5}}} \qquad \text{Eq. 2.8}$$

Where, ε_m is the mean strain increment, V_p, the particle impact velocity, ρ_p is the particle density, C_p, the target specific heat, T_m, the melting point of target material and the H_t is the static hardness of the metal or alloy [37].

Reddy & Sundararajan, 1986 conducted experiments using a constant velocity of 40 m/s at impact angles of 30º, 60º, and 90º on two ductile materials. Based on the SEM micrograph they suggested that lip formation and fracture are the fundamental erosion mechanisms. It has been reported that the erosion rate corresponds to the following relation:

$$\boldsymbol{\varepsilon_{vp}\ \alpha\ \frac{L^3\ \Delta\Omega_m}{\Omega_C}} \qquad \text{Eq. 2.9}$$

Where ε_{vp} is the erosion rate, L is the depth of deformation, $\Delta\Omega_m$ is the mean strain increment induced by each impact, and Ω_c is the critical strain for the onset of lip formation [38].

2.3.2.3 Fatigue Models

Based on low cycle fatigue theory, at normal impacts, it is assumed that the element of volume will be lost once it acquires a critical strain. I. M. Hutchings, 1981 model predicted that the erosion rate will be inversely related to product of the target yield strength and its fracture strain. While at oblique impacts, Ratner, 1981 equated volume undergoing heavy deformation with the volume of crater. The model predicted a velocity exponent of 3.5.

The velocity exponent (n) of the model was predicted as 3.

$$E = 0.033 \frac{\alpha \rho \sigma^{1/2} v^3}{\varepsilon_c^2 P^{3/2}} \quad \text{Eq. 2.10}$$

Where, E is the erosion rate, α is the fraction of the volume of the indentation, which depends on the indentation geometry, the impact velocity and the target material, ρ is the density of target material, σ is the dynamic hardness of target material, ε is the erosion ductility, and P is the constant pressure [39,40].

2.3.2.4 Adiabatic Shear Induced Spalling Models

The removal of chunks of the target material is the result of intersection of shear bands formation in the crippled volume beneath the crater. The formation of adiabatic shear bands requires a critical strain and deformation. Therefore, their formation is obvious in high strength (low work hardening) alloys. If this mechanism prevails, the angle of maximum weight loss will appear at higher angles than for those metals where shear is more homogeneous. This model provides an attractive explanation for the experimental observation that in hardened steels the angle of maximum erosion shifts from roughly 20° to near 90° as the hardness is increased to Rockwell C 60 and above [1].

2.3.3 Factors Affecting Solid Particle Erosion

Erosion is seen to be influenced by several parameters like erodent properties, target material properties, fluid properties, impact conditions, and temperature effect. Particle properties have a significant repercussion on solid particle erosion. The effect of each factor like size, density, shape, and hardness has been investigated by researchers separately. Some of them are discussed below:

2.3.3.1 Erodent Shape and Size

The shape and size of the erodent particle have an important role in determining the extent of erosion. The characteristics of the erodent govern the way it interacts with the target surface and the mechanisms through which erosion occurs. Q. B. Nguyen et al., 2019 evaluated the size effect of abrasive sand particles on the erosion characteristics of stainless steel (SS304). The study utilized abrasive sand particles of different size i.e., 50, 80, 150, 350, 450, and 700 μm exhibiting an experimental angularity with an average value of 0.58. The main component of the sand material was aluminum oxide, comprising approximately 95% of the composition, followed by TiO_2 at around 3%, SiO_2 at 1.3%, F_2O_3 at 0.16%, and CaO at 0.5%. The erosion rate (measured in kg per impact), the depth of erosion, and the surface roughness all increase with increase in the particle size [41].

Lin et al., 2018 examined the influence of erodent particle size (75, 150, 300, and 600 μm) and shape (angular, semi-round and round) on the erosion of stainless steel 316 at different impact angles of 15°, 30°, 45°, 60°, 75° & 90° and at a constant particle velocity of 95 m/s and reported an increase in erosion with increasing particle size. It has been attributed to the higher plastic deformation with increasing size and consecutive material removal [42].

Torres et al., 2013 studied the erosive wear of AISI 420 stainless steel under solid particle impact using angular silicon carbide (SiC) and steel round grits with a particle size of 400-420 μm (Mesh 60) at four different incident angles i.e., 30°, 45°, 60°, and

90° with the silicon carbide particles traveling at an approximate speed of 24±2 m/s and a flow rate of 21±2.5 g/min, while the steel round grit particles flowing at a rate of 48.5±3.5 g/min. The results indicated a higher mass loss in the specimens subjected to angular silicon carbide particles compared to those attacked by round steel grit. The difference in severity has been attributed to the presence of deep wear scars, indicating a typical cutting mechanism as the primary wear mechanism [43].

2.3.3.2 Properties of Erodent Material

The density and hardness are the key properties of the erodent responsible for erosion. A higher density erodent has higher kinetic energy and creates more impact force causing enhanced erosion rate.

Feng et al., 1999 carried out on solid particle erosion tests on four different materials (glass, alumina, WC–7% Co, and 304 stainless steels) using seven distinct erodent (steel shot, glass beads, silica, alumina, tungsten carbide, silicon carbide, and diamond particles) encompassing a wide range of particle diameters (63 to 1000 μm), velocities (33 m/s to 99 m/s), and impact angles ranging from 30° to 90°. It has been indicated that kinetic energy, particle size and the relative hardness &toughness of erodent control the erosion rate of brittle materials namely, glass and alumina whereas shape and kinetic energy of are more important for ductile materials. It has also been reported that there is no significant effect of hardness of erodent on erosion [44].

Levy & Chik, 1983 conducted experiments to study the effect of erodent composition, hardness-strength and shape factor on the erosive wear of AISI 1020 carbon steel by carrying out tests at a velocity of 80 m/s and two angles of impingement (30° and 90°)

with erodent particles having Vickers' hardness ranging from 115 to 3000 kgf/mm^{-2} and particle size ranging from 180 to 250 μm. The erosion rate has been found to increase with increasing particle hardness until reaching a certain threshold and the erosion rate remained constant beyond a Vickers' hardness of 700 kgf/mm^{-2}. The constant erosion rate after certain hardness has been attributed to the strength of the particles, which enables them to endure the impact without breaking up [45].

2.3.3.3 Erodent Flow rate

Studies have revealed that the flow rate of the erodent has a significant effect on the erosion behavior of the materials. Lin et al., 2018 investigated the effect of flow rate (0.53 g/s and 2.83 g/s) on the erosion behavior of SS316 steel using silica sand and glass beads as the erodent materials and reported a larger material loss at the lower sand low rate (0.53 g/s) compared to the higher sand flow rate (2.83 g/s). The phenomenon has been attributed to the sand blanketing effect, wherein particles collide and shield the target from incoming particles [42].

Liebhard et al., 1991 examined the effect of shape, mass, size, impact velocity, and feed rate on the erosivity of particle streams on 1018 steel using spherical glass beads and angular SiC as the erodent with two different feed rates, 0.6 g/min, and 6 g/min and observed a greater mass loss at lower feed rates compared to higher feed rates. This observation was attributed to the high number of collisions occurring between particles at lower feed rates, which obstructed the incoming particles from effectively impacting the target surface [46].

2.3.3.4 Impact Velocity

The impact velocity plays a crucial role in determining the erosion rate of a material. When a solid particle impacts a surface with a certain velocity, it transfers kinetic energy to the surface upon impact. This energy is then dissipated through various mechanisms, resulting in the removal or degradation of material from the surface. The higher the impact velocity, the greater the kinetic energy transferred to the surface, leading to a more significant erosion effect. The erosion rate has been shown to be directly proportional to impact velocity (V^n). The value of 'n', typically varies from 1.6 to 2.6 [47].

Sharma et al., 2015 examined the influence of martensite volume fraction on the erosive wear of dual-phase steels using silica sand as the erodent material at various velocities (45, 72, and 95 m/s) and impingement angles (30°, 60°, and 90°) and demonstrated an increase in erosion rate with increase in impact velocity. It has been attributed to the increased kinetic energy at higher velocities [48].

Islam & Farhat, 2014 conducted erosion tests on API X42 pipeline steel at different impact velocities and impact angles of 36 m/s, 47 m/s, 56 m/s and 81 m/s at 30°, 45°, 60°, and 90°, respectively, using aluminum oxide as erodent and reported an increase in erosion rate increasing particle impact velocity. The erosion has been indicated to occur by plastic deformation, fracture, ploughing and metal cutting [49].

Divakar et al., 2005 investigated the erosion behavior of austenitic stainless steel at impact velocities of 20 and 32 m/s using silica sand as erodent and observe a higher erosion rate at higher velocity. It has been attributed to the greater impact energy of particles at higher velocities, which subsequently resulted in higher erosion rates [50].

2.3.3.5 Impact Angle

The impact angle has a significant influence on the erosion rate of materials. When an erosive medium, such as a liquid or gas carrying solid particles, impinges on a material surface, the angle at which it strikes plays a crucial role in determining the rate of material removal or erosion. Several studies have been conducted to observe the variation of impact angle with erosion rate [34,51–56].

V. B. Nguyen et al., 2014 investigated the effect of impact angle on the erosion on 304 stainless steel (304SS) by carrying out tests at angles ranging 10° to 90° and reported an increase in erosion rate with the increase in impact angle from 10° to 40° and a decrease thereafter till 90°. The results revealed that the most severe erosion occurred at an impact angle of 40°. This can be attributed to the observed erosion mechanism. At low impact angles, micro-plowing was the dominant mechanism, whereas, at higher impact angles, the erosion process transitioned to indentation-induced plastic deformation [51].

Gercekcioglu et al., 2009 studied the effect of impact angle on the erosive wear of low carbon and low alloyed AISI 1020, AISI 1040, AISI 4140, and AISI 8620 steels. At different impingement angles of 15, 30, 45, 60, 75, and 90° and at a constant velocity of 30 m/s using the G40 particles as erodent. It has been reported that the erosive wear rate

of steels increased with decreasing impact angle and the observed behaviour has been explained with the help of erosion mechanisms at different impact angles. The micro cutting and ploughing of material have been stated as the dominant material removal mechanisms at lower impact angles whereas ploughing has been found to be dominant at higher impact angles [57].

Rodriguez et al., 2009 investigated the erosion wear behavior of AISI H13 steel and AISI 4140 steel under a sand blast type rig using silica sand as the erodent material at impact angles ranging from 10° to 90°, air drag pressures of 0.689 and 1.38 bar (10 and 20 psi respectively), impact speeds ranging from 70 to 107.0 ms^{-1}. The erosion rate has been shown to vary with impact angle depending on the hardness of the target material. For impact angles of 10° and 20°, the amount of wear was higher at lower hardness values whereas no significant changes were found in the amount of wear despite the increase in hardness for impact angles of 30° and 40°. However, for impact angles of 60°, 75° and 90° the amount of wear was higher for harder target material. The behaviour has been explained on the basis of the dependence of cutting action of particles on the angle of impingement [58].

2.3.3.6 Properties of Target Material

The properties of the target material have also been reported to affect the erosion rate. Numerous studies have indicated that higher material hardness caused reduced erosion rate. Laguna-Camacho et al., 2013 evaluated the performance of AISI 304, 316, and 420 SS in the erosion process. The materials have been tested at a particle velocity of 24 m/s

with an abrasive flow rate of 150 g/min impacted at 30°, 60°, and 90°. In 420 SS, the erosion rate reaches its peak at a 30° impact angle, whereas for AISI 304 and 316 SS, the highest erosion rate occurs at a 60° impact angle. This has been attributed to the observed material removal mechanism. The plastic deformation characterized by pitting and cutting action has been observed in 420SS. In comparison, AISI 304 and 316 SS showed wear damage, much like brittle fractures with the detachments of large fragments [59].

Islam et al., 2015 investigated the effect of microstructure on the erosion of AISI 1018 and AISI 1080 steel for variable impact velocity (36, 47, 56 and 81 m/s) and impact angles (30°, 45°, 60° and 90°). At low impact angle (30°), AISI 1018 exhibits better erosion resistance than AISI 1080 steel. Ploughing, metal cutting, and delamination are the controlling mechanisms. It has been observed that at a low impact angle, AISI 1018 steel exhibits more embedded particles resulting in better erosion resistance [60].

2.3.3.7 Temperature

The erosion rate has been found to be influenced by the surrounding temperature. At higher temperatures, the material undergoes softening, resulting in changes to its mechanical and microstructural properties. This, in turn, reduces its resistance to erosive forces, making it more susceptible to material removal. Liu et al., 2021 investigated the erosion behavior of dual-phase steels at different temperatures and found that a decrease in erosion resistance with increasing temperature due to the reduced strength and hardness of the steel at elevated temperatures [61].

J. Xu et al., 2018 investigated the effect of temperature on the erosion behavior of dual-

phase steel under various impact angles and reported an increase in erosion rate with increasing temperature and angle of impact. The increased erosion rate has been attributed to a reduction in strength and hardness of the steel at elevated temperatures. A change in erosion mechanism from plowing to cutting with increasing temperature has also been observed by them [62]. He et al., 2002 investigated the erosion behavior of dual-phase steel under different temperatures and particle velocities and found that the erosion rate increased with increasing temperature and particle velocity. The increased rate of erosion has been ascribed to the decreased hardness and toughness of the steel at high temperatures. It has been indicated that the effect of temperature on solid particle erosion of dual-phase steel is complex and depends on several factors, including the microstructure and properties of the steel, the type and size of the particles, the velocity of the particles, and the temperature of the system. However, the general trend is that the erosion resistance decreases with increasing temperature due to the reduced strength and hardness of the steel at elevated temperatures [63].

2.3.4 Mechanisms of Erosion

Erosion by solid particle impact involves several forces having different source of origin. Neighbouring particles may apply contact forces whereas gravity may also be important-t in some situations. However, the main force on an erosive particle, which is primarily responsible for its deceleration from initial impact velocity, is typically the contact force exerted by the surface. The extent of wear in erosion depends on the number and mass of individual particles striking the surface, and on their impact velocity. Mechanisms of erosive wear may involve both plastic deformation and brittle

fracture. Erosion of metals usually encompasses plastic flow, whereas brittle materials experience predominantly either flow or fracture depending on the impact conditions.

2.3.4.1 Erosive Wear by Plastic Deformation

I.M. Hutching proposed a model for erosion by a single hard particle impact on a soft surface at normal incidence assuming that the particle does not deform and that the problem can be analysed quasi-statically by ignoring dynamic effects. Hence, the only force supposed to be acting is the contact force exerted by the surface with an additional assumption that the deformation of the surface is perfectly plastic, with a constant indentation pressure (hardness) H. In such a case, the material displaced from the indentation can undergo different possibilities: (i) it may be accommodated by elastic deformation of material away from the indentation, (ii) it may form a rim of plastically deformed material around the indentation, or (ii) it may be removed in some way as wear debris.

The mass of material removed may be given by Eq. 2.11 given below. I. M. Hutchings & Winter, 1975

$$\boldsymbol{mass\ of\ material\ removed} = \boldsymbol{\rho \frac{mU^2}{2H}} \qquad \text{Eq. 2.11}$$

Where ρ is the density of the material being eroded, H is the indentation pressure hardness, U is the impact velocity, and m is the mass of particle [1].

I M Hutchings and Winter examined the interaction between a hard particle and the surface of a ductile as well as brittle materials at different angles and illustrated that the ductile metals usually display peak erosion at a shallow impact angle (curve a), while brittle materials often demonstrate maximum wear at normal incidence (Fig. 2.4 (a)). At

30° impact angle three basic types of impact damage occur as illustrated in Fig. 2.5. The surface gets deformed by the rounded particle by ploughing, displacing material to the side and in front of the particle (Fig. 2.5 (a)). The continuous impacts on neighbouring areas lead to the detachment of heavily-strained material from the rim of the crater or from the lip at its end. This type of deformation encompasses both the ploughing and wedge-forming modes of abrasion. However, the deformation triggered by an angular particle is dependent on the angle at which it attacks the surface, and on the backward or forward rolling of particle rolls during contact. Type-I cutting mode occurs when particle rolls forwards impacting the surface and raises materials into a pronounced lip, which is susceptible to get removed by subsequent nearby impacts. The opposite rotation of these angular particles results in Type-II cutting, which occurs for only a limited range of particle geometries and impact orientations (Fig. 2.5). The material gets detached in the form of chips by the plastic rupture only after undergoing numerous cycles of plastic deformation and after severely work hardening [64].

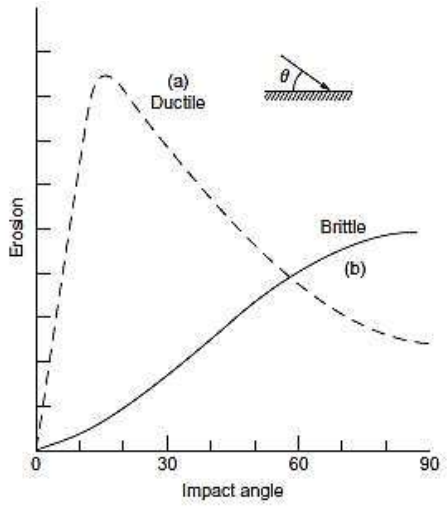

Figure 2.4 Typical dependence of erosion rate on impact angle for ductile and brittle materials [1]

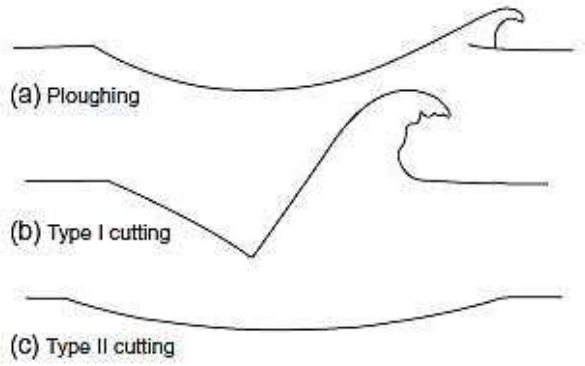

Figure 2.5 The impact direction was from left to right. (a) Ploughing deformation by a sphere; (b) type I cutting by an angular particle, rotating forwards during impact; (c) type II cutting by an angular particle, rotating backwards during impact [1]

The effect of erosion on ductile materials arises from various physical properties, with plastic deformation being the most prominent. A low impingement angle tends to favor abrasion-like wear processes as the particles tend to track across the worn surface after impact. Conversely, a high impingement angle leads to wear mechanisms typical of erosion. At a low impact angle (i.e. 15° to 45°), the particles impact and leave the surface forming ploughing and lip formation marks. Whereas at intermediate impact between 45° to 75°, removal of chips takes place by cutting. However, at higher impact angles i.e., 75° to 90°, material usually piles around the craters, which get removed with the subsequent impacts

The shape of the abrasive particles influences the pattern of plastic deformation around each indentation and the proportion of the material displaced from each indentation which forms a rim or lip. More rounded particles lead to less localized deformation, and

more impacts are required to remove each fragment of metal chips. An increased impact angle has a similar effect. In the extreme case of spherical particles at normal incidence, material is removed only after neighbouring impacts have imposed many cycles of plastic deformation, and the surface looks very different from one eroded by angular particles.

The dependence of erosive wear of metals with the particle impact velocity is often expressed in the form

$$\boldsymbol{E \propto U^n} \qquad \text{Eq. 2.12}$$

The velocity exponent *n* is nearly always greater than the value of 2.0 and often lays around 2.4 for ductile metals at impact angles close to that of maximum erosion.

2.3.4.2 Erosive Wear by Brittle Fracture

The removal of material from the surface of target material takes place by the formation and intersection of cracks in case of brittle fracture caused by the impinging particles. However, there is always some plastic flow around the point of contact of an angular particle even though the detachment of the wear debris is by brittle fracture. The extent of cracking due to particle impact is most severe when the impact direction is normal to the surface, and erosion under these conditions is then most rapid as depicted in Fig. 2.4, curve (b) which shows the dependence of erosion on impact angle for a typical case where wear occurs by brittle fracture.

For the angular particles which are more commonly encountered in practice, material is assumed to be removed by the intersection of lateral cracks with each other and with the

surface. One model estimates the contact force exerted on the particle during impact by assuming that the pressure resisting penetration is the quasi-static hardness of the surface (as in the model leading to equation 2.4). The contact force is then used in a semi-empirical analysis to predict the extent and depth of the lateral cracks formed, and hence the volume of material removed by a single impact. This predicts a volume erosion (volume removed per unit mass of erodent particles), E/ρ given by

$$\frac{E}{\rho} = r^{0.7} U^{2.4} \frac{\sigma^{0.2} H^{0.1}}{K_c^{1.3}} \qquad \text{Eq. 2.13}$$

Where *Kc* is the fracture toughness of target material, *H* is the hardness target material, *U* is the impact velocity, *r* is the particle size, and *σ* is the density of the erodent particles.

2.4 EROSIVE WEAR OF STEELS

The erosion behavior of steels has been investigated by several researchers [65–71]. Chowdhury et al., 2022 studied the erosion effect on SS 420, SS 304, SS 316, and SS 201 stainless steel to observe the cumulative effect of Al_2O_3, Fe_2O_3, SiC solid particles at different impact angles and velocities and reported that the erosion was more severe at a 60° impact angle and it decreased gradually until a 90° impact angle [68].

Lv & Yang, 2022 investigated the effect of the impact stress on the surface of AISI 1020 at various impingement angles, velocities and particle sizes and reported that the occurrence of gouging in erosion pits and plastic extrusion higher impact angles and micro-cutting and furrow lips at a smaller angle. It has also been indicated that an increasing in impact velocity of the cuttings leads to a significant increase in the

maximum equivalent stress, accumulation of material at the front of the erosion pit, and deformation lip height. It has been observed that the maximum material accumulation and deformed lip occur at a 45° impact angle [69].

Okonkwo et al., 2015 observed the influence of impact angles (30° to 90°) and particle velocities (20 m/s to 80 m/s) on the erosion mechanisms of AISI 1018 steel and reported that the ploughing mechanism was dominant at 90° whereas the low angle metal cutting, embedment of particles, micro-cutting, pitting and ploughing were the governing erosion mechanisms at lower impingement angles [70].

Sharma et al., 2015 investigated the erosive wear of DP steels containing different amounts of martensite (36%, 59% and 72%) at different impact angles (30°, 60° and 90°) and velocities (45, 72 and 95 m/s) using silica sand as erodent and reported that the erosion resistance increases with increasing martensite volume fraction. The erosion rate of dual-phase steels was observed to be higher when subjected to 30° impact angle and 95 m/s impact velocity due to the collective effect of sliding and impact from silica particles [48].

Islam & Farhat, 2014 conducted erosion tests on API X42 pipeline steel at various impact velocities (36 m/s, 47 m/s, 56 m/s and 81 m/s) and impact angles (30°, 45°, 60°, and 90°), respectively, using aluminum oxide as erodent under a high mean abrasive feed rate of 160 g/min. The erosion rate was observed to decrease with increasing angle of impact and increase with increasing particle impact velocity by plastic

deformation, fracture, ploughing and metal cutting [49].

Hussain et al., 2012 conducted erosion tests on AISI 444, AISI 439 and AISI 304 and low carbon steel AISI 1010 at room temperature using silica sand of sizes 150-300 μm, at different velocities (40-85 m/s) and impingement angles (15-90°) and reported that the maximum erosion rate for AISI 444, AISI 439 and AISI 304 occurred at about 30° impingement angle while the same for AISI 1010 took place at 45° angle, The material removal was observed to have occurred by the lip or platelet formation in all the steels [72].

Gercekcioglu et al., 2009 examined the erosive wear of low carbon and low alloyed AISI 1020, AISI 1040, AISI 4140, and AISI 8620 steels at different impingement angles of 15, 30, 45, 60, 75, and 90 and at a constant velocity of 30 m/s using G40 particles as erodent and reported an increase in erosion rate with decreasing angle of impact [57].

Laura et al., 1985 investigated the effect of microstructure (spheroidite, pearlite, martensite, and tempered martensite), particle velocity (40-100 m/s), and angle of impingement (10-90°) on the erosion of AISI-SAE 1078 and 10105 steels and reported the maximum erosion rate for spheroidite and pearlite microstructures at an impingement angle of 40° with a ductile mode of erosion at all velocities. However, a brittle mode of failure was observed for martensite and tempered martensite with increasing velocity at different angles of impingement [34].

2.5 CORROSION

Corrosion is a “Physico-chemical interaction, usually of an electrochemical nature, between a metal and its environment which results in changes in the properties of the metal and which may often lead to impairment of the function of the metal, the environment, or the technical system of which these form a part” [73]. The primary cause of corrosion is the reaction of metal atoms with substances in the environment, such as oxygen, water, acids, or salts. This reaction leads to the formation of corrosion products, which are typically oxides, hydroxides, or sulfides of the metal. The corrosion process can be accelerated by factors like humidity, temperature, pollutants, and the presence of dissimilar metals in contact with each other.

2.5.1 Types of Corrosion

Corrosion can take various forms, depending on the metal and the specific environmental conditions. Some common types of corrosion include: Galvanic Corrosion, Uniform Corrosion, Crevice Corrosion, Pitting Corrosion, Intergranular Corrosion, Erosion Corrosion, and Stress Corrosion Cracking.

2.5.1.1 Galvanic Corrosion

A galvanic cell is a cell where reactions occur spontaneously at two electrodes when they are connected by a conductor [74]. Dissimilar metals with different electrochemical potentials act as galvanic cells where the active one corrodes when coupled together. The potential difference between the two drives preferential corrosion of one or the other. EMF series (thermodynamic) and galvanic series (kinetic) could be used for

prediction of this type of corrosion. Micro galvanic corrosion is important for multi-phase microstructures and DP steels.

2.5.1.2 Uniform Corrosion

Uniform corrosion is one of the most common types of corrosion which occurs with the equal distribution of anode and cathode zones at the surface. Corrosion occurs more or less evenly, or rather uniformly, across the surface of the metal. It occurs in compositionally uniform metals like cast irons and steels and results in an even surface depletion, as seen in atmospheric corrosion of many metals [75].

2.5.1.3 Crevice Corrosion

Crevice corrosion refers to a localized form of attack on a metal that occurs in the narrow gap or crevice between two adjoining surfaces, which can be between two metals or between a metal and a non-metal material. Several factors come into play in influencing the occurrence and severity of crevice corrosion as suggested by Betts & Boulton, 1993. Typically, the corrosion is limited to a specific area on one of the metals. This type of corrosion is often triggered by concentration gradients, which arise from the presence of ions or oxygen. The accumulation of chlorides within the crevice accelerates the damage caused by crevice corrosion [76]. The major factors influencing crevice corrosion are mentioned below:

- Materials: alloy composition, metallographic structure
- Geometrical feature of crevices, surface roughness
- Environmental conditions such as pH, oxygen concentration, halide concentrations, temperature.

- Metal to metal or metal to nonmetal type.

2.5.1.4 Pitting Corrosion

Pitting corrosion is a localized phenomenon confined to smaller areas and the formation of micro-pits can be significantly damaging. Pitting factor i.e., the ratio of the deepest pit to the average penetration is often used to evaluate severity of pitting corrosion which is usually observed in passive metals and alloys. Concentration cells involving oxygen gradients or ion gradients are responsible for initiating pitting through generation of anodic and cathodic areas. Chloride ions are damaging to the passive films and can make pit formation auto-catalytic. Pitting tendency can be predicted through measurement of pitting potentials

2.5.1.5 Intergranular Corrosion

Localized attack at or nearer to grain boundaries in a metal or alloy can be termed as intergranular corrosion. Generally, the Impurities & precipitation at grain boundaries and depletion of an alloying element (added to resist corrosion) in the grain-boundary area contribute to intergranular corrosion.

2.5.1.6 Erosion Corrosion

Erosion corrosion refers to the degradation of metals and alloys caused by the interaction between their surfaces and corrosive fluids while experiencing relative movement and the extent of the movement determines the level of abrasion that occurs. This type of corrosion is identifiable by the presence of grooves and surface patterns that exhibit a distinct directionality. Common examples of materials susceptible to erosion corrosion are stainless alloy pump impellers and condenser tube walls.

Any equipment exposed to fluid flow with movement is prone to erosion corrosion. Many failures related to erosion corrosion can be attributed to impingement, known as "impingement attack." High-velocity impingement in specific applications can lead to erosion corrosion, such as in steam condenser tubes, slide valves in petroleum refineries at high temperatures, inlet pipes, cyclones, and steam turbine blades [77].

2.5.1.7 Stress Corrosion Cracking

Stress corrosion cracking (SCC) occurs when there is a combination of a corrosive environment and tensile stress, leading to material failure. The occurrence of stress cracking in various alloys is influenced by the specific corrosive environment they are exposed to. The incidence of stress corrosion cracking (SCC) is influenced by several key variables, including the composition of the solution, the metal or alloy composition, and structure, as well as the levels of stress and temperature. When SCC failures happen, the crack morphology typically exhibits brittle fracture with the presence of inter- or trans-granular cracking. The time before crack initiation is reduced under higher stresses. Tensile stresses, whether they are applied, residual, or thermal stresses, play a significant role, and they must reach sufficient threshold levels to initiate stress cracking [78].

2.5.2 Factors affecting corrosion of Materials

(i) Reactivity of metal

The reactivity of a metal plays a significant role in its susceptibility to corrosion. Metals that are higher in the reactivity series, such as iron, zinc, and aluminum, are more prone

to corrosion. These metals have a strong tendency to react with oxygen and moisture in the environment, forming metal oxides. For instance, iron reacts with oxygen to form iron oxide, commonly known as rust. In contrast, metals lower in the reactivity series, like gold, platinum, and silver, exhibit low reactivity and are more resistant to corrosion [79].

(ii) Strain in metal

Strain refers to the deformation or stress experienced by a metal. Corrosion is more likely to occur in areas where the metal has undergone mechanical strain, such as cuts, bends, or welds. Strain can cause localized stress concentration, disrupting the protective oxide layer on the metal's surface. This disruption weakens the metal's resistance to corrosion, making the strained areas more susceptible to corrosive attacks [80].

(iii) Presence of impurities

The presence of impurities in a metal significantly affects its corrosion behavior. The impurities act as initiation sites for corrosion, leading to localized corrosion or pitting and also promote the formation of galvanic cells when two dissimilar metals are in contact, accelerating the corrosion process. Additionally, impurities can also alter the microstructure of metals and affect the stability of protective oxide layers. In the presence of impurities, the corrosion resistance of metals decreases, making it more prone to corrosion [81].

(iv) Presence of electrolyte

An electrolyte is a medium that facilitates the movement of ions. The presence of an electrolyte is essential for electrochemical corrosion to occur. Electrolytes can be in the form of moisture, water, saltwater, or other aqueous solutions. When a metal is in

contact with an electrolyte, it can undergo electrochemical reactions, leading to corrosion. For example, in saline water (an electrolyte), metals readily corrode due to the presence of chloride ions that enhance the electrochemical corrosion process [82].

(v) Conditioning gases and moisture

Corrosion can be influenced by the presence of certain gases and moisture in the environment. Gases such as carbon dioxide (CO_2), sulfur dioxide (SO_2), and sulfur trioxide (SO_3) can react with moisture in the air to form acidic compounds. These acidic gases, along with moisture, create a corrosive environment that accelerates metal corrosion. For instance, carbon dioxide dissolved in water forms carbonic acid, which can corrode metals like iron. Similarly, the presence of sulfur dioxide and sulfur trioxide can lead to the formation of sulfuric acid, a highly corrosive substance [80].

(vi) Environmental Conditions

Environmental conditions such as temperature, humidity, and pH levels can further impact corrosion. For example, high temperatures and high humidity can accelerate corrosion rates. Furthermore, the composition and structure of the material itself, including its surface finish, protective coatings, and alloying elements, can also affect its corrosion resistance [79].

2.5.4 Corrosion of DP Steels

The phenomenon of corrosion in DP steels has been studied by a number of authors and effect of factors such as martensite volume fraction, morphology of martensite on the corrosion behaviour of DP steels has been reported [61,74,83–88]. Chen et al., 2021,

investigated micro-galvanic corrosion behavior of DP steels containing fresh and tempered martensite using 0.1 M NaCl aqueous solution and opined that both tempered and fresh martensite serve as a micro-cathode to promote the anodic dissolution of adjacent ferrite matrix. The corrosion of DP steel has been shown to occur in two stages, (i) increased corrosion due to successive emergence of cathodic tempered and fresh martensite phases, and (ii) decrease in corrosion rate due to martensite of separation which weakens the micro-galvanic effect [83].

Abdo et al., 2020 investigated the influence of Cl^- ions on the electrochemical corrosion behavior of dual-phase (DP) rebar compared to conventional rebar by carrying out electrochemical measurements using simulated concrete pore solutions with varying Cl^- ion concentrations. The analysis of potentiodynamic polarization and electrochemical impedance spectroscopy measurements indicated that DP rebar exhibits excellent passivity, leading to enhanced corrosion resistance and greater strength when compared to ordinary rebar. The study also indicated that the dual-phase nature of DP steel, comprising ferrite and martensite, contributed to its superior corrosion resistance in various electrolyte solutions [84].

Hao et al., 2020 investigated the corrosion behavior of DP steels containing (53 to 71%) martensite volume fraction (MVF) using electrochemical measurements performed on three-electrode system composed of the working electrode, platinum electrode, and saturated calomel electrode (SCE), potentiodynamic polarization and electrochemical impedance spectroscopy (EIS) and compared the results with commercial AH32 steel using 3.5% NaCl solution as electrolyte. It has been reported that an increase in the

intercritical annealing temperature leads to the enhanced galvanic effect between ferrite and martensite and accelerates the corrosion rate of DP steels. DP750 steel having 53 % martensite content has been reported to show the highest resistance to corrosion. This has been attributed to the change in the amount of martensite amount with the increasing temperature leading to potential difference between martensite and ferrite phases, and the formation of galvanic cells between ferrite and martensite [89].

Kumar et al., 2019 analyzed the corrosion behavior of DP steels containing 32 to 100% martensite using open-circuit potential (OCP) measurement, Potentiodynamic polarization, and electrochemical impedance spectroscopy (EIS) techniques in 3.5% NaCl. It has been reported that corrosion depends on the galvanic susceptibility between martensite (cathode) and ferrite (anode), and self-corrosion propensity of each phase and the competition between self-corrosion and galvanic corrosion governs the corrosion resistance behavior of DP steels [86].

Fushimi et al., 2013 explored the corrosion characteristics of high-purity dual-phase steel containing ferrite and martensite phases in a 0.1 M sulfuric acid solution using both macro- and micro-electrochemical methods. It has been reported that the dual-phase steel exhibited a non-uniform corrosion due to the galvanic coupling between its microstructure, as well as the self-corrosion of each phase. It has also been suggested that the hydrogen evolution reaction on galvanic-coupled martensite accelerated the iron dissolution reaction of ferrite and led to a approximately three times greater corrosion

rate of martensite than that of ferrite due to its self-corrosion in the acidic environment [74].

Bhagavathi et al., 2011 also examined the corrosion behavior of plain low carbon dual-phase (DP) steels with varying volume fractions of martensite by conducting potentiodynamic polarization and immersion tests using 3.5% NaCl solution. The corrosion rate of dual-phase steels has been observed to be lower than that of heat-treated ferrite-pearlite steel and enhanced corrosion resistance in dual-phase steels has been attributed to their unique microstructural features. Soleimani et al., 2011 [90], carried out spheroidization heat treatment and intercritical annealing to investigated the effect on the mechanical properties and corrosion behavior of CK45 medium carbon steel and reported that an increase in spheroidization time resulted in a decrease of strength and hardness but with simultaneous improvement in ductility and corrosion resistance. It has also been indicated that an increase in holding time at intercritical annealing temperature resulted in increased martensite content with a decrease in corrosion resistance [87].

2.6 FORMULATION OF THE PROBLEM

From the above review of the available literature, it is obvious that most of the studies conducted in the past have been restricted to the correlation between the microstructure and the mechanical properties of the DP steels. A critical review of literature pertaining wear of steels indicates that a number of studies have been carried out to examine the sliding and abrasive wear behavior as well as the corrosion of plain carbon steels, steels having fine pearlite, coarse pearlite, martensite or bainite, stainless steels and DP steels.

However, only a few investigations have been conducted to understand the erosion and corrosion behavior of the DP steels. Most of these studies have been carried out with fixed annealing times, at which the austenite volume fraction reaches almost an equilibrium value. Some kinetic studies have also been carried out on the effect of intercritical annealing time to elucidate the mechanism of austenite formation, but little effort has been made to study the effect of intercritical annealing time on the mechanical properties of the DP steel, which, in turn, affect its behavior under erosive or corrosive conditions. During iso-thermal annealing, the austenite phase grows into the ferrite regions after consuming pearlite areas. If quenching is done before equilibrium is attained at the intercritical temperature, the martensite volume fraction progressively increases with increasing intercritical annealing time. This change in the martensite volume fraction influences the mechanical properties of the dual phase steels and it has marked influence on the wear as well as the corrosion behavior of dual phase steels.

Though DP steels have been extensively studied in order to achieve an optimum combination of mechanical properties required for structural applications, but the erosive and corrosive behavior of medium carbon DP steel have hardly drawn any attention. Nonetheless, there are several interesting features in DP steels, which render them suitable for applications involving erosion and corrosion.

The present study is motivated by a need to unravel the erosive wear behavior of plain carbon DP steels having varying amounts of the martensite in the microstructure. The study also intends to evaluate the effect of the martensite content on the performance of

DP steels under corrosive environments. The martensite content in the microstructure could be varied by changing the time of intercritical annealing at a fixed temperature in order to understand its effect on the erosion as well as corrosion behavior of DP steels.

The variation of mechanical properties of DP steels with increasing volume fraction of martensite could be determined. This will help in explaining the erosive wear characteristics of these steels as it strongly depends on the mechanical properties, especially the hardness of the material. The change in fracture behavior of the DP steels with increasing volume fraction of martensite could be determined by examining the fractured surfaces of tensile specimens under Scanning Electron Microscope (SEM) and the change in the nature of fracture with the martensite volume fraction. Also, considering that all of these steels are produced from the same composition, it may also be quite fascinating to examine how the erosion and corrosion characteristics of these steels vary with different phase fractions. Thus, the purpose of this research is to evaluate the erosive wear performance of normalized (N) steel, dual phase (DP) steels and fully martensitic steels (FMS) at various impact angles and velocities. The eroded and corroded surfaces of the steels and the nature of the wear marks after erosion and surface degradation after corrosion has been studied to confirm the nature of erosive wear and corrosion mechanisms. The subsurface structure of the worn specimens has been examined to identify subsurface deformation and micro crack formation and their contribution to the observed wear. In short, the study aims to explore the operating mechanisms of material removal and the effect of microstructure the erosive wear as well as the corrosion behavior of N steel, DP steels and FMS.

2.7 OBJECTIVES OF THE STUDY

The present study has been conducted with the following objectives.

1. To develop DP steels having varying fractions of martensite volume fraction through intercritical annealing heat treatment.

2. To determine the effect of martensite volume fraction on the mechanical properties and to establish a correlation between microstructure and mechanical properties.

3. To explore the effect of microstructure, impingement angle and impact velocity on erosive wear of medium carbon steel, DP steels and fully martensitic steel.

4. To establish the mechanism of material in steels having the different microstructure vis-à-vis a combination of impact angle and velocity.

5. To examine the corrosion behavior of normalized and DP steels in 3.5% NaCl solution.